Pergamon

Int. J. Solids Structures Vol. 35, No. 36, pp. 5033–5050, 1998

Printed in Great Britain
0020-7683/98/$ - see front matter

PII: S0020-7683(97)00269-2

DISLOCATION BEHAVIOURS AHEAD OF CRACK TIP

T. C. WANG
LNM, Institute of Mechanics, Chinese Academy of Sciences, Beijing 100080, P.R. China

(*Received* 15 *February* 1996; *in revised form* 2 *September* 1997)

Abstract—In this paper, a unified mechanics model for dislocation nucleation, emission and dislocation free zone is proposed based on the Peierls framework. Three regions are identified ahead of the crack tip. The emitted dislocations within the plastic zone in the form of an inverse pile up are treated as discrete elastic edge dislocations. Between that zone and the cohesive zone immediately ahead of the crack tip, there is a dislocation free zone. With the stress field and the dislocation density field in the cohesive zone, respectively, expressed in the first and second Chebyshev polynomial series, and the opening and slip displacements in trigonometric series, a set of nonlinear governing equations are obtained which take into account for the interaction between the emitted dislocations and cohesive zone and the nonlinear interaction between sliding displacement and the opening displacement. After discretization, the governing equations are transformed into a set nonlinear algebraic equations which are solved with Newton–Raphson Method. The results of calculation for pure shearing and combined tension and shear loading after dislocation emission are given in detail. Finally, the process of dislocation nucleation and emission on a pair of symmetric slip planes of angle α with respect to the crack plane under pure mode I load is analysed. The equilibrium positions and the number of emitted dislocation are determined. Several possible competition behaviors of dislocation emission vs cleavage are revealed.

1. INTRODUCTION

This paper is concerned with the dislocation behaviors near a crack tip. The process of dislocation emission from a stressed crack has been observed in numerous experiments (see e.g. Ohr, 1985; Horton and Ohr, 1982; Chiao and Clark 1989). As pointed out by Ohr (1985), a dislocation will be generated at the crack tip if the applied stress is sufficiently large. Once generated, the dislocation will move out of the crack tip area, leaving behind a dislocation free zone. In their pioneering work, Rice and Thomson (1974) presented a dislocation emission model to characterize the plastic shear at crack tip and developed a quantitative criterion for ductile vs brittle behaviour.

Recently Rice (1992), Schoeck (1991), Rice *et al.* (1992) and Beltz and Rice (1991) have reanalyzed the Rice–Thomson criterion on the basis of the Peierls model. For the mode II case, Rice (1992) presented an exact solution for the loading at that the nucleation instability was developed and identified a solid-state parameter, the unstable stacking energy γ_{us}, which characterizes the resistance to dislocation nucleation.

A new approach was developed by Wang (1995) with a slightly modified Rice's concept. Both the dislocation nucleation and emission from the crack tip were analyzed based on Peierls framework. The calculation clearly shows that there is a well defined region of fairly "perfect" crystal between the emitted dislocation and the crack tip area, which can be treated as the dislocation free zone.

This paper presents a mechanics model to analyse the dislocation behaviours ahead of the crack tip, such as the dislocation nucleation, dislocation emission and dislocation free zone and to quantify the interactions between the emitted dislocations in the plastic zone and the distributed dislocation in the cohesive zone and the nonlinear interaction between sliding displacement and the opening displacement.

2. THE DESCRIPTION OF THE MODEL

Suppose that the crack faces are contained within one of the possible slip planes in a crystal. For a general loading Beltz and Rice (1991) proposed a generalized constitutive relation:[1]

$$\tau_x = \tau_{\max} A_0(\Delta_y) \sin\left(2\pi \frac{\Delta_x}{b}\right)$$

$$\sigma_y = \sigma_{\max} B_0(\Delta_x) \frac{\Delta_y}{L} e^{1-\frac{\Delta_y}{L}} \tag{1}$$

where

$$A_0(\Delta_y) = \left(1+\frac{\Delta_y}{L}\right) e^{-\frac{\Delta_y}{L}} \tag{2}$$

$$B_0(\Delta_x) = 1 - q\sin^2\left(\pi \frac{\Delta_x}{b}\right), \quad q = \frac{\gamma_{us}}{2\gamma_s} \tag{3}$$

where γ_s is the surface energy, γ_{us} the unstable stacking energy, and L is the scaling length of the Thomas–Fermi screening length.

As shown in Fig. 1, Δ_x denotes the relative displacement of two atomic planes adjacent to the slip plane. With δ_x defined as the slip displacement discontinuity on a mathematical cut coincident with the slip plane, we have

$$\Delta_x = \delta_x + \frac{\tau_x}{\mu} h \tag{4}$$

where h is the interplanar spacing.

δ_x can be taken as the plastic shearing along slip plane. Suppose for a perfect crystal, there will be no inelastic shearing until the resolved shear stress τ reaches the critical shear stress τ_0. Hence eqn (4) becomes

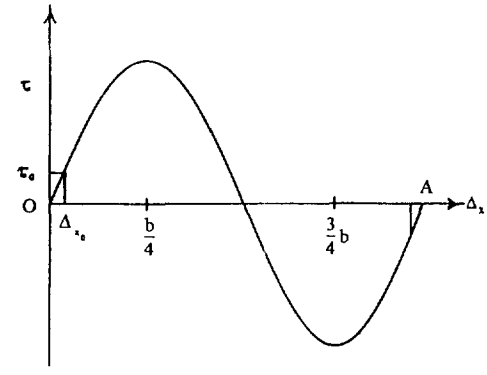

Fig. 1. Shear stress vs shear displacement on a slip plane.

[1] Only the case of $r = 0$ is considered here.

$$\Delta_x = \begin{cases} \delta_x + \dfrac{\tau_x}{\mu} h, & \tau_x > \tau_0 \\ \dfrac{\tau_x}{\mu} h, & \tau_x \leqslant \tau_0 \end{cases} \tag{5}$$

Let Δ_y denote the relative atomic separation across the slip plane, which can similarly be expressed as

$$\Delta_y = \begin{cases} \delta_y + \dfrac{\sigma_y}{E} h, & \sigma_y > \sigma_0 \\ \dfrac{\sigma_y}{E} h, & \sigma_y \leqslant \sigma_0 \end{cases} \tag{6}$$

where δ_y is the opening displacement discontinuity on the slip plane, σ_0 the critical tension stress is the proportional limit in pure tension for a perfect crystal, and E the Young's modulus of the crystal.

Figure 2 shows a plane strain or plane stress semi-infinite crack, which lies on the negative x axis with its slip at $x = 0$. Let R_1 denote the length of the cohesive zone for the slip displacement and R_2 the length of the decohesive zone for the opening displacement. Beyond R_1, there is no discontinuity for the slip displacement, and beyond R_2, discontinuity of the opening displacement vanishes.

The emitted dislocations are located at positions x_i $(i = 1, 2, \ldots, n)$ within the plastic zone. The interval $[R, x_n]$ can be considered as the dislocation free zone, where the $R = \max\{R_1, R_2\}$.

3. BASIC FORMULAS

According to Wang (1995) and Loo (1978), the traction on the cohesive zone ahead of the crack tip is

$$\sigma_y - i\tau_{xy} = \sigma_y^{(0)} - i\tau_{xy}^{(0)} + \frac{2\mu}{(\kappa+1)\pi i}\int_0^R \frac{\sqrt{\tau}\hat{b}(\tau)}{\sqrt{x}(x-\tau)}\,\mathrm{d}\tau + \frac{2\mu b}{(\kappa+1)\pi i}\sum_{i=1}^{n}\frac{\sqrt{x_i}}{\sqrt{x}(x-x_i)} \tag{7}$$

where $\sigma_y^{(0)}$, $\tau_{xy}^{(0)}$ are the singular stress field, and $\hat{b}(\tau) = b_x(\tau) + ib_y(\tau)$, b is the magnitude of the Burgers vector of the emitted dislocations in the plastic zone, n is the number of the emitted dislocations.

Equation (7) can be represented as

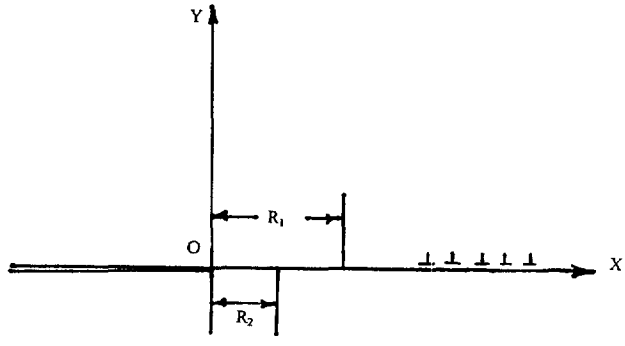

Fig. 2. Cohesive zone, decohesive zone ahead of a crack tip, dislocation free zone and emitted dislocations.

$$\frac{2\mu}{(\kappa+1)\pi}\left\{\int_0^{R_1}\frac{\sqrt{\tau}b_x(\tau)}{x-\tau}\mathrm{d}\tau+b\sum_{i=1}^{n}\frac{\sqrt{x_i}}{(x-x_i)}\right\}=\sqrt{x}[\tau_{xy}-\tau_{xy}^{(0)}] \tag{8a}$$

$$\frac{2\mu}{(\kappa+1)\pi}\int_0^{R_2}\frac{\sqrt{\tau}b_y(\tau)}{x-\tau}\mathrm{d}\tau=\sqrt{x}[\sigma_y-\sigma_y^{(0)}] \tag{8b}$$

Introduce following nondimensional quantities:

$$t_1=\frac{x}{R_1},\quad t_2=\frac{x}{R_2},\quad s_1=\frac{\tau}{R_1},\quad s_2=\frac{\tau}{R_2} \tag{9}$$

and let

$$F_1(t_1)=\sqrt{t_1}b_x(x)\cdot\frac{\mu}{\kappa+1}$$

$$g_1(t_1)=\sqrt{t_1}[\tau_{xy}-\tau_{xy}^{(0)}] \tag{10}$$

$$F_2(t_2)=\sqrt{t_2}b_y(x)\frac{\mu}{\kappa+1}$$

$$g_2(t_2)=\sqrt{t_2}[\sigma_y-\sigma_y^{(0)}] \tag{11}$$

Then eqn (8) becomes

$$-\frac{2}{\pi}\left\{\int_0^1\frac{F_1(s_1)\,\mathrm{d}s_1}{s_1-t_1}+\frac{\mu b}{(\kappa+1)R_1}\sum_{i=1}^{n}\frac{\sqrt{t_{1i}}}{(t_{1i}+t_1)}\right\}=g_1(t_1)$$

$$-\frac{2}{\pi}\int_0^1\frac{F_2(s_2)\,\mathrm{d}s_2}{s_2-t_2}=g_2(t_2) \tag{12}$$

The singularity of the dislocation density $\hat{b}(x)$ is less than $(1/\sqrt{x})$ at the crack tip, while the dislocation density $\hat{b}(x)$ vanishes at the end of the cohesive zone.

With the variable translations: $t_1=\frac{1}{2}(1+\cos\theta)$, and $t_2=\frac{1}{2}(1+\cos\varphi)$ functions $F_1(t_1)$ and $F_2(t_2)$ can be expressed as the following sine series:

$$F_1(t_1)=\frac{1}{2}\sum_{m=1}^{\infty}\alpha_m\sin m\theta,\quad t_1=\frac{1}{2}(1+\cos\theta)\quad 0\leqslant\theta\leqslant\pi$$

$$F_2(t_2)=\frac{1}{2}\sum_{m=1}^{\infty}\beta_m\sin m\varphi,\quad t_2=\frac{1}{2}(1+\cos\varphi)\quad 0\leqslant\varphi\leqslant\pi \tag{13}$$

eqn (13) can be rewritten as:

$$F_1(t_1)=\frac{1}{2}\sqrt{1-\eta_1^2}\cdot\sum_{m=1}^{\infty}\alpha_m U_m(\eta_1)$$

$$F_2(t_2)=\frac{1}{2}\sqrt{1-\eta_2^2}\cdot\sum_{m=1}^{\infty}\beta_m U_m(\eta_2)$$

$$\eta_1=\cos\theta,\quad \eta_2=\cos\varphi \tag{14}$$

where $U_m(\eta)$ is the second Chebyshev polynomial

$$U_m(\eta) = \frac{\sin m\theta}{\sin\theta}, \quad \eta = \cos\theta, \quad m = 1, 2, \ldots$$

Substituting eqn (14) into eqn (13) and using the following formula

$$\frac{1}{\pi}\int_{-1}^{1} \frac{\sqrt{1-\xi^2}\,U_m(\xi)\,\mathrm{d}\xi}{\xi-\eta} = -T_m(\eta) \tag{15}$$

$$T_m(\eta) = \begin{cases} \cos m\theta, \eta = \cos\theta, & -1 \leqslant \eta \leqslant 1 \\ [\eta - \sqrt{\eta^2-1}]^m, & \eta > 1 \\ [\eta + \sqrt{\eta^2-1}]^m, & \eta < -1 \end{cases} \tag{16}$$

one obtains

$$g_1(t_1) = \sum_{m=1}^{\infty} \alpha_m T_m(\eta_1) + \frac{2\mu b}{(\kappa+1)\pi R_1} \sum_{i=1}^{n} \frac{\sqrt{t_{1i}}}{(t_1 - t_{1i})}$$

$$g_1(t_2) = \sum_{m=1}^{\infty} \beta_m T_m(\eta_2) \tag{17}$$

where $T_m(\eta)$ is the generalized first Chebyshev polynomial, and

$$t_{1i} = \frac{x_i}{R_1}, \quad \eta_1 = 2t_1 - 1, \quad \eta_2 = 2t_2 - 1$$

The opening displacement and sliding displacement take the form

$$\delta_x + i\delta_y = \int_x^R \hat{b}(\tau)\,\mathrm{d}\tau \tag{18}$$

Using eqn (11) and eqn (15), we obtain

$$\frac{\mu}{(\kappa+1)}\delta_x = \frac{R_1}{4}\sum_{m=1}^{\infty} \alpha_m V_m(\theta) + \frac{\mu}{(\kappa+1)} nb \quad 0 \leqslant x \leqslant R_1 \tag{19}$$

$$\frac{\mu}{(\kappa+1)}\delta_y = \frac{R_2}{4}\sum_{m=1}^{\infty} \beta_m V_m(\varphi), \quad 0 \leqslant x \leqslant R_2 \tag{20}$$

$$V_m(\theta) = \frac{\sin(m-\frac{1}{2})\theta}{m-\frac{1}{2}} - \frac{\sin(m+\frac{1}{2})\theta}{m+\frac{1}{2}} \tag{21}$$

The singular stress field can be expressed as

$$\sigma_y^{(0)} + i\tau_{xy}^{(0)} = \frac{K}{\sqrt{2\pi r}} \tag{22}$$

here $K = K_{\mathrm{I}} + iK_{\mathrm{II}}$ is the complex stress intensity factor.

Substituting eqn (22) into eqns (10) and (11), we obtain

$$\tau_{xy} = \frac{1}{\sqrt{t_1}}\left[g_1(t_1) + \frac{K_{II}}{\sqrt{2\pi R_1}}\right]$$
$$\sigma_y = \frac{1}{\sqrt{t_2}}\left[g_2(t_2) + \frac{K_I}{\sqrt{2\pi R_2}}\right] \tag{23}$$

The shear stress and the normal stress at the crack tip are finite. Hence from eqn (23) one can get

$$\frac{K_{II}}{\sqrt{2\pi R_1}} = -\sum_{m=1}^{\infty} \alpha_m \cos m\pi + \frac{2\mu b}{(\kappa+1)\pi R_1}\sum_{i=1}^{n}\frac{1}{\sqrt{t_{1i}}}$$
$$\frac{K_I}{\sqrt{2\pi R_2}} = -\sum_{m=1}^{\infty} \beta_m \cos m\pi \tag{24}$$

In the cohesive zone eqn (23) can be expressed as

$$\tau_{xy} = \frac{1}{\sqrt{t_1}}\sum_{m=1}^{\infty}\alpha_m(\cos m\theta - \cos m\pi) + \frac{2\mu b}{(\kappa+1)\pi}\sum_{i=1}^{n}\frac{\sqrt{x}}{\sqrt{x_i}(x-x_i)}$$
$$\sigma_y = \frac{1}{\sqrt{t_2}}\sum_{m=1}^{\infty}\beta_m(\cos m\varphi - \cos m\pi) \tag{25}$$

The above stress fields must be balanced with the cohesive stress fields of eqn (1). Similarly in the plastic zone, the shear stress exerted on the ith emitted dislocation is

$$\tau_{xyi} = \frac{K_{II}}{\sqrt{2\pi x_i}} + \frac{1}{\sqrt{t_1}}\sum_{m=1}^{\infty}\alpha_m T_m(\eta_{1i}) + \frac{2\mu b}{(\kappa+1)\pi}\left\{-\frac{1}{2x_i} + \sum_{j=1}^{n}\frac{\sqrt{x_j}}{\sqrt{x_i}(x_i-x_j)}\right\} \tag{26}$$

In this equation the first term on the right-hand side is the K_{II} field produced by the external loading, the second term is due to the distributed dislocations in the cohesive zone, the third term is due to its own image stress and the summation term accounts for the stress fields of all other emitted dislocation in the plastic zone and their images. Using eqn (24), eqn (26) can be rewritten as

$$\tau_{xyi} = \frac{1}{\sqrt{t_{1i}}}\sum_{m=1}^{\infty}\alpha_m(T_m(\eta_{1i}) - \cos m\pi) + \frac{2\mu b}{(\kappa+1)\pi}\left\{\frac{1}{2x_i} + \sum_{j=1}^{n}\frac{\sqrt{x_i}}{\sqrt{x_j}(x_i-x_j)}\right\} \tag{27}$$

As suggested by Li (1981), Li and Thomson (1986), the shear stress acting on the ith dislocation in the plastic zone should be equal to the lattice friction τ_f. Thus, we have

$$\tau_{xyi} = \tau_f, \quad i = 1, \ldots, n \tag{28}$$

Assume the emitted dislocations pile up behind an obstacle which is provided by the exited dislocation structure, grain boundary, etc. Hence instead of the first equation of the equation set (28), we should add a constraint equation

$$x_1 = x_{ob} \tag{29}$$

eqns (25), (28) and (29) are the governing equations.

4. CALCULATION METHODS AND RESULTS

The unknown coefficients $\{\alpha_m\}$, $\{\beta_m\}$ and $\{x_i\}$ are chosen as the basic unknown quantities. The infinite series in eqns (13) and (17) can be approximated with a sufficient degree of accuracy by the corresponding truncated series.

The cohesive zone $0 \leqslant x \leqslant R_1$ is discretized into M elements, which vary in size along the region. The nodal points are given by the following expression

$$X_i = \frac{1}{2} R_1 \left[1+\cos\left(\frac{(i-1)\pi}{M}\right)\right] \tag{30}$$

Similarly the decohesive zone $0 \leqslant x \leqslant R_2$ is divided into N elements. The nodal points are given by the formula

$$X_j^* = \frac{1}{2} R_2 \left[1+\cos\left(\frac{(j-1)\pi}{N}\right)\right] \tag{31}$$

The governing equations are then transformed into a set of nonlinear algebraic equations.

$$\begin{aligned}
&\sum_{k=1}^{M} a_{ik}\alpha_k + \frac{2\mu b}{(\kappa+1)\pi}\sum_{j=1}^{n}\frac{\sqrt{X_i}}{\sqrt{x_j}(X_i-x_j)} - \tau_{\max}A_0(\Delta_{yi})\sin\left(2\pi\frac{\Delta_{xi}}{b}\right) = 0, \quad i = 1,2,\ldots,M \\
&\sum_{k=1}^{N} b_{jk}\beta_k - \sigma_{\max}B_0(\Delta_{xj}^*)\frac{\Delta_{yj}^*}{L}e^{1-\frac{\Delta_{yj}^*}{L}} = 0, \quad j = 1,2,\ldots,N \\
&\frac{1}{\sqrt{t_{1k}}}\sum_{m=1}^{\infty}\alpha_m(T_m(\eta_{1k})-\cos m\pi) + \frac{2\mu b}{(\kappa+1)\pi}\left\{\frac{1}{2x_k}+\sum_{l=1}^{n}\frac{\sqrt{x_k}}{\sqrt{x_l}(x_k-x_l)}\right\} = \tau_f \quad k = 2,\ldots,n
\end{aligned} \tag{32}$$

where

$$a_{ik} = \frac{[\cos(k\theta_i)-\cos(k\pi)]}{\sqrt{T_{1i}}}$$

$$\theta_i = \frac{(i-1)\pi}{M}, \quad T_{1i} = \frac{X_i}{R_1}, \quad t_{1k} = \frac{x_k}{R_1} \tag{33}$$

$$b_{jk} = \frac{[\cos(k\varphi_j)-\cos(k\pi)]}{\sqrt{T_{2j}}}, \quad \varphi_j = \frac{(j-1)\pi}{N}, \quad T_{2j} = \frac{X_j^*}{R_2} \tag{34}$$

Δ_{xi}, Δ_{yi} are the shearing and opening displacements at $X_i = R_1(1+\cos\theta_i)/2$, Δ_{xj}^*, Δ_{yj}^* are the shearing and opening displacements at $X_j^* = R_2(1+\cos\varphi_j)/2$.

Equations (32) and (29) are solved by the Newton–Raphson method.

It is worth noting that the convergency of the Newton–Raphson method for solving the eqns (32) and (29) is dependent on the choice of the initial values of $\{\alpha_m^0\}$, $\{\beta_m^0\}$ and $\{x_i^0\}$. If the initial values of $\{\alpha_m^0\}$, $\{\beta_m^0\}$ and $\{x_i^0\}$ are "good" enough, then the iterating convergence is guaranteed after five to ten iterations, otherwise the iterating process may be divergent.

In order to get a set of suitable values of $\{x_i^0\}$, we neglect the cohesive zone. The eqn (28) becomes

$$\frac{K_{II}}{\sqrt{2\pi x_i}} + Ab\left\{-\frac{1}{2x_i} + \sum_{j=1}^{n} \frac{\sqrt{x_j}}{\sqrt{x_i}(x_i - x_j)}\right\} = \tau_f \tag{35}$$

where $A = 2\mu/(\kappa+1)\pi$.

The local stress intensity factor is given by

$$\frac{K_{II}^{tip}}{\sqrt{2\pi b A}} = \frac{K_{II}}{\sqrt{2\pi b A}} - \sum_{i=1}^{n} \frac{\sqrt{b}}{\sqrt{x_i}} \tag{36}$$

For a set of given values of (x_{ob}/b), n, $(K_{II}^{tip}/\sqrt{2\pi b A})$ and (τ_f/A), the eqns (35) and (29) can be easily solved by Newton–Raphson method. The iterating convergence is very quick and is not sensitive to the initial values of $\{x_i^0\}$.

On the other hand, using the approach by Wang (1995) one can easily obtain the coefficients $\{\alpha_m\}$ and $\{\beta_m\}$ for the case of $N_d = 0$ and a given value of $(K_{II}^{tip}/\sqrt{2\pi b A})$. Then the calculated coefficients $\{\alpha_m\}$ and $\{\beta_m\}$ and the values of $\{x_i\}$ obtained by solving eqns (35) and (29) can be chosen as the initial values of the $\{\alpha_m^0\}$, $\{\beta_m^0\}$ and $x_i^0\}$ for solving eqns (32) and (29).

Most calculations in this paper were carried out with five digits of accuracy for the stress fields in the cohesive zone.

Calculation results

The calculations were carried out with materials parameters

$$\frac{h}{b} = 1, \quad \frac{L}{b} = 0.4, \quad \nu = 0.3, \quad \frac{\tau_f}{A} = 0.005 \quad \text{and} \quad M = 180 \quad \text{and} \quad N = 180$$

Pure shear loading

The critical stress intensity factor K_{IIc} for dislocation emission is given by Rice (1992)

$$K_{IIe} = \sqrt{\frac{2\mu\gamma_{us}}{(1-\nu)}} = 0.667\sqrt{2\pi b A}$$

When the applied load is increased, the stress intensity factor K_{II} will increase. As the mode II stress intensity factor reaches the critical value K_{IIe}, the first dislocation is fully nucleated at the crack tip, then emitted from the crack tip along the slip plane and stopped at a distance r_1. The local stress intensity factor K_{II}^{tip} are decreased. As the applied load increases again the local stress intensity factor K_{II}^{tip} also increases. When the local stress intensity factor K_{II}^{tip} reaches the critical value K_{IIe} again, the second dislocation is fully nucleated at the crack tip then emitted along the slip plane and stopped at distance r_2, which results in decrease of the local stress intensity factor. The sequence was repeated, until the nth dislocation were emitted.

Figure 3 shows the slip displacement profiles for pure shear loading after ten and twenty dislocation emissions for the case of

$$\frac{R_1}{b} = 228.5, \quad \frac{x_{ob}}{b} = 5000, \quad \frac{\tau_0}{\mu} = 0.01, \quad \text{and} \quad \frac{\tau_{max}}{\mu} = 0.159$$

For $N_d = 10$, the local stress intensity factor $K_{II}^{tip}/\sqrt{2\pi b A} = 0.663$ which is a little bit smaller than K_{IIe}.

Figure 4 shows the positions of the emitted dislocations. The shear stress τ_{xy} distribution ahead of the crack tip is shown in Fig. 5.

In these figures, the solid lines with white small circles are the results for $N_d = n = 10$, while the solid lines with black small triangles are the results for $N_d = n = 20$. The corresponding stress intensity factors are $(K_{II}/\sqrt{2\pi b A}) = 0.818$ and 0.972, respectively.

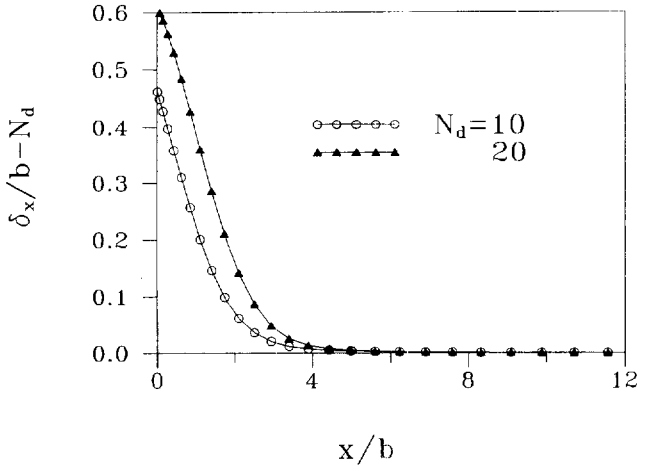

Fig. 3. Shear displacement profiles for a pure mode II crack after 10 and 20 dislocation emissions for the case of

$$\frac{R_1}{b} = 228.5, \quad \frac{x_{ob}}{b} = 5000, \quad \frac{\tau_0}{\mu} = 0.01, \quad \text{and} \quad \frac{\tau_{max}}{\mu} = 0.159.$$

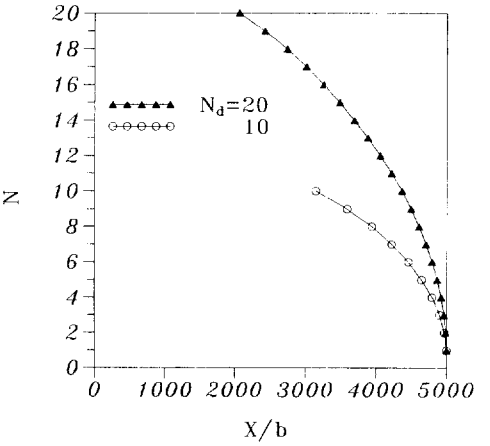

Fig. 4. Position of the emitted dislocations for the case of that of Fig. 3.

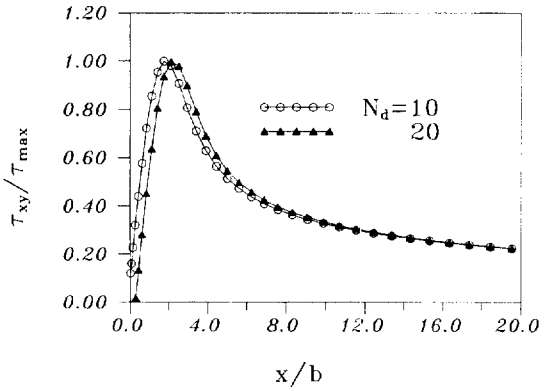

Fig. 5. Shear stress distributions along the cohesive zone for a pure mode II crack after dislocation emissions for the case of that of Fig. 3.

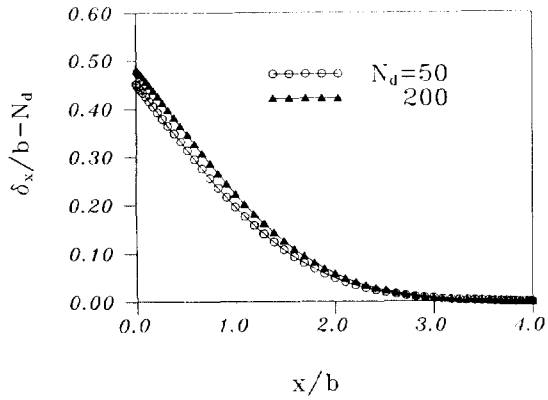

Fig. 6. Slip displacement profiles for a pure mode II crack after 50 and 200 dislocation emissions for the case of

$$\frac{R_1}{b} = 4, \quad \frac{x_{ob}}{b} = 3000, \quad \frac{\tau_0}{\mu} = 0.1, \quad \text{and} \quad \frac{\tau_{max}}{\mu} = 0.170.$$

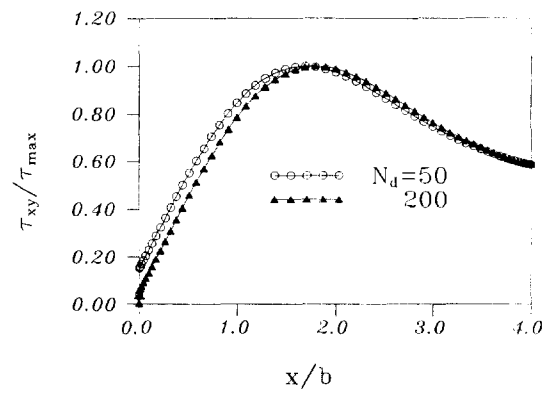

Fig. 7. Shear stress distributions along the cohesive zone for a pure mode II crack after dislocation emissions for the case of that of Fig. 6.

These figures show that, as the number N_d of the emitted dislocation increases, the shear stress at the crack tip decreases while the shear displacement at the crack tip minus N_d increases for a given value of R_1.

The slip displacement profiles for pure shear loading after fifty and two hundreds dislocation emissions for the case of $(R_1/b) = 4$, $(x_{ob}/b) = 3000$, $(\tau_0/\mu) = 0.1$ and $(\tau_{max}/\mu) = 0.170$ are shown in Fig. 6. The shear stress and normal stress distributions ahead of the crack tip are shown in Fig. 7. The positions of the emitted dislocations are plotted in Fig. 8.

In these figures, the results for $N_d = n = 50$ are denoted by the solid lines with white small circles, while the solid lines with black small triangles are designed for the results for $N_d = n = 200$. The corresponding stress intensity factors are $(K_{II}/\sqrt{2\pi bA}) = 1.84$ and 5.97, respectively.

It can be seen that the number N_d of the emitted dislocations has small effect on the shear stress distribution near the crack tip due to the emitted dislocations are far away from the crack tip, but has great effect on the stress intensity factor. The stress distribution near the crack tip is controlled by the local stress intensity K_{II}^{tip}, which is mainly determined by the parameter R_1.

But we should emphasis that for a given parameter R_1 the deformation state near the crack tip will become unstable if the number N_d of the emitted dislocations is large enough

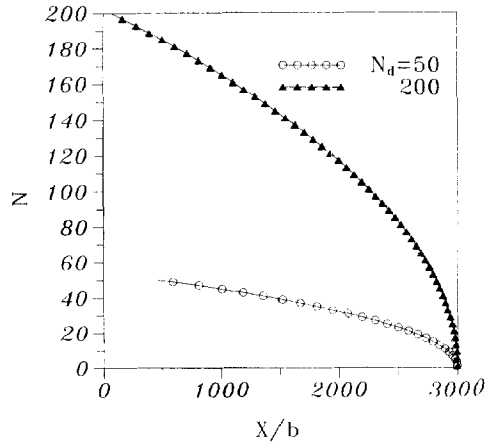

Fig. 8. Positions of the emitted dislocations for the case of Fig. 6. For $N_d = 200$, only half of the emitted dislocation is plotted on the figure.

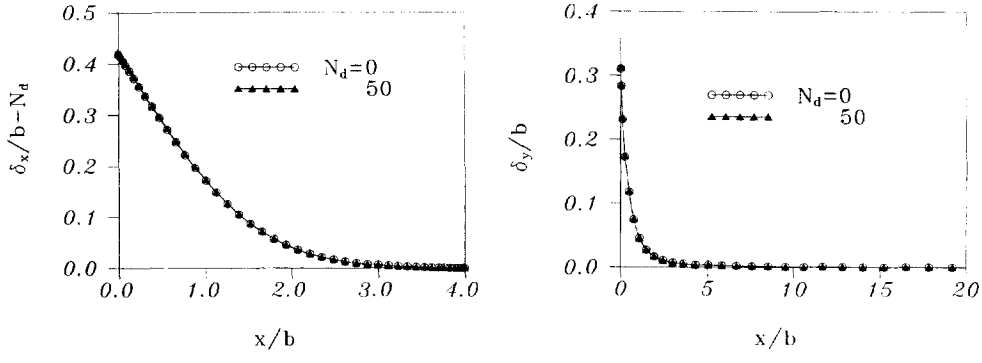

Fig. 9. Displacement profiles for a combined mode crack after 50 dislocation emissions from the crack tip for the case of

$$\frac{R_1}{b} = 4, \quad \frac{R_2}{b} = 100, \quad \frac{x_{ob}}{b} = 3000, \quad \frac{\tau_0}{\mu} = 0.1, \quad \frac{\tau_{max}}{\mu} = 0.170,$$

$$\frac{\sigma_0}{E} = 0.008, \quad \frac{\sigma_{max}}{E} = 0.0766.$$

(i.e. the applied stress intensity factor K_{II} is big enough), which results in continuously dislocation emission and completely dislocation shielding on the crack tip. In such cases, whole interval $[0, x_{ob}]$ is transformed to the plastic zone and the dislocation free zone vanishes.

Combined tensile and shear loading

The results for a general combined shear and tension loading after fifty dislocation emissions from the crack tip are given in Figs 9 and 10. Figure 9 shows the slip and opening displacement profiles for the case of $(R_1/b) = 4$, $(R_2/b) = 100$,

$$\frac{x_{ob}}{b} = 3000, \quad \frac{\tau_0}{\mu} = 0.1, \quad \frac{\tau_{max}}{\mu} = 0.170, \quad \frac{\sigma_0}{E} = 0.008, \quad \frac{\sigma_{max}}{E} = 0.0766$$

The stress fields ahead of the crack tip are shown in Fig. 10.

In these figures, the solid lines with black small triangles are results for $N_d = n = 50$. The solid lines with white small circles are the results before dislocation emission. The

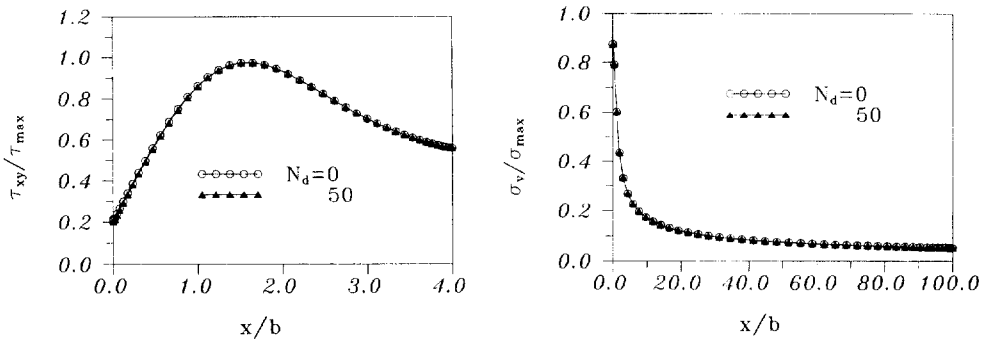

Fig. 10. Shear and normal stress distributions ahead of the crack tip for a combined mode crack after 50 dislocation emissions for the case of Fig. 9.

corresponding stress intensity factors are $(K_I/\sqrt{2\pi bA}) = 0.903$ and $(K_{II}/\sqrt{2\pi bA}) = 1.84$, respectively.

5. RESULTS OF ELASTIC THEORY

Above calculations clearly show that the stress fields near the crack tip are controlled by the local stress intensity factors and the inelastic behaviours in the cohesive zone only has slight effect on the positions of the emitted dislocations and the applied stress intensity factors when the emitted dislocations are far away from the crack tip. Hence if we are interested in the global behaviours, we can neglect the cohesive zone.

This section only deals with the elastic interaction of the emitted dislocations with the infinite crack, which is controlled by eqns (35) and (36).

The eqns (35) and (36) have been derived early by Li and coworkers (1981, 1982). In a series of computer studies, Li and his coworkers (1991, 1992) assume that each dislocation moves according to a power law of the shear stress exerted on it minus a lattice friction stress.

In the present study we give up Li's assumption and directly solve the eqns (35), (36) and (29) using the Newton–Raphson method.

Effects on the applied stress intensity factor

The applied stress intensity factor K_{II} vs the number of the emitted dislocations is plotted in Fig. 11 for the case of $(K_{II}^{tip}/\sqrt{2\pi bA}) = 0.685$, $(x_{ob}/b) = 3000$ and $(\tau_f/A) = 0.005$.

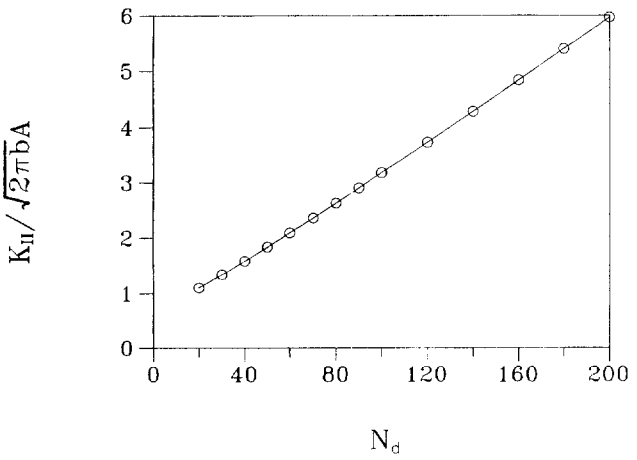

Fig. 11. Applied stress intensity factor K_{II} vs the number N_d of the emitted dislocations with parameters $(K_{II}^{tip}/\sqrt{2\pi bA}) = 0.685$ and $(\tau_f/A) = 0.005$.

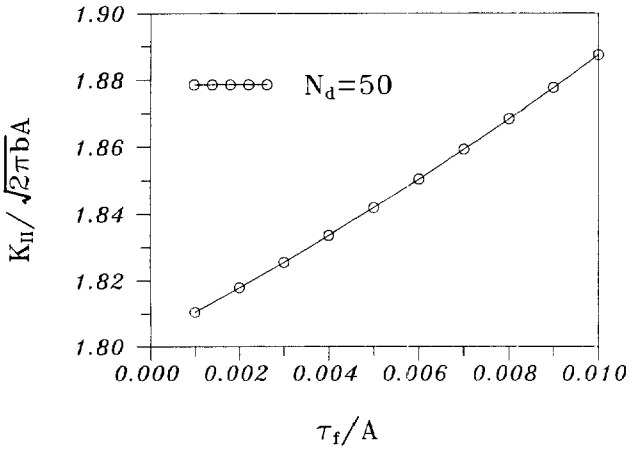

Fig. 12. The relationship of the applied stress intensity factor K_{II} vs τ_f/A for the case of $(K_{II}^{tip}/\sqrt{2\pi bA}) = 0.685$ and $N_d = 50$.

The applied stress intensity factor K_{II} is nearly proportional increase as the total number N_d of the emitted dislocations increases. The applied stress intensity factor K_{II} is also increased when the lattice friction stress increases as shown in Fig. 12.

Inverse pileup dislocation array

Direct TEM observations on the thin sheet specimens by Ohr and his coworkers (1985, 1982) have shown that the emitted dislocations in the plastic zone are often in the form of an inverse pileup. The dislocation density near the crack tip is remarkably high and decreases away from the crack tip. Since the TEM observations are made on the pure single crystals. Hence the dislocation array rarely interact with the obstacles. Thus the constraint eqn (29) should take out from the governing equations. We only need to solve eqns (35) and (36).

Figure 13 shows the positions of the emitted dislocations for the case of $(K_{II}^{tip}/\sqrt{2\pi bA}) = 0.685$ and $(\tau_f/A) = 0.015$. The emitted dislocation distributions for the case of $(K_{II}^{tip}/\sqrt{2\pi bA}) = 0.685$ and $(\tau_f/A) = 0.005$ are shown in Fig. 14. From these figures one can see that the emitted dislocations in the plastic zone are really in form of an inverse pileup and the emitted dislocations are located much more away from the crack tip compared with that of Figs 4 and 8.

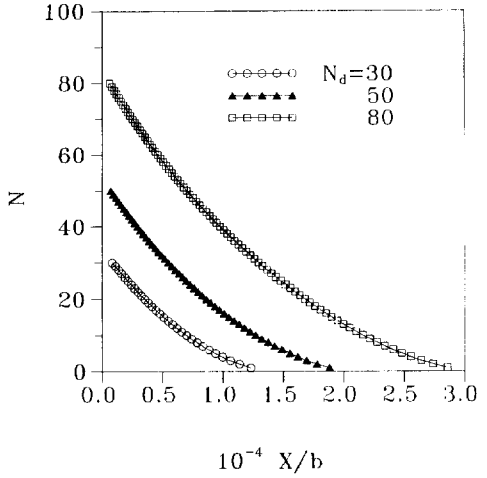

Fig. 13. The distributions of the emitted dislocations for the case of $(K_{II}^{tip}/\sqrt{\pi bA}) = 0.685$ and $\tau_f/A = 0.015$.

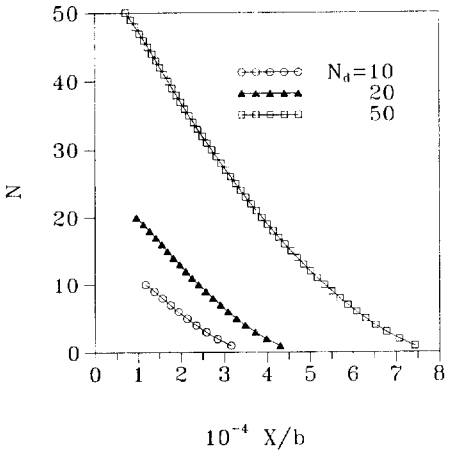

Fig. 14. The positions of the emitted dislocations for the case of $(K_{II}^{tip}/\sqrt{2\pi bA}) = 0.685$ and $\tau_f/A = 0.005$.

6. DISLOCATION NUCLEATION AND EMISSION ALONG INCLINED PLANES

Now we consider the process of dislocation nucleation and emission on a pair of symmetric slip planes of angle α with respect to the crack plane as shown in Fig. 15. The crack configuration is remotely loaded by pure mode I stress intensity factor K_I. The integer N_d denotes the total number of emitted dislocation in one arm of the symmetric slip planes. The equilibrium positions of the emitted dislocation are denoted by r_i, $i = 1, 2, \ldots, N_d$.

Assume the emitted dislocation on each arm pile up behind an obstacle, which is located at r_{ob}. Hence we have a constraint equation

$$r_1 = r_{ob}$$

The dislocation nucleation and emission are treated as a pure shear process. The governing equations for the problem are similar with that of Section 3. An incipient static distribution δ_r of sliding discontinuity across a pair of symmetric slip plane develops in the cohesive zones. The equilibrium equation for shear along upper slip plan in the cohesive zone is

$$\tau[\Delta_r] = \tau_{r\theta}^{(0)}(r) + A\int_0^R g(r,s)b_r(s)\,ds + Ab\sum_{j=1}^{n} g(r,r_j) \tag{37}$$

where $A = 2\mu/(\kappa+1)\pi$, $n = N_d$, and $\tau_{r\theta}^{(0)}(r)$ is the singular shear stress due to the applied stress intensity factor K_I

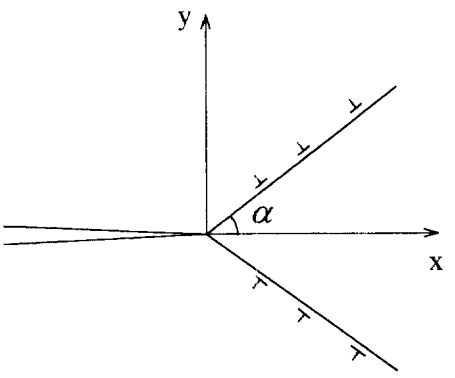

Fig. 15. A pair of symmetric slip planes emanate from the crack tip.

$$\tau_{r\theta}^{(0)}(r) = \frac{K_I b}{2\sqrt{2\pi r}} \sin\alpha \cos\frac{\alpha}{2}$$

where b is the magnitude of the Burgers vector along the inclined slip planes.

The second term in the right hand side of eqn (37) is the shear stress produced by the distributed dislocation in the upper and lower cohesive zones. The third term is the shear stress contributed by the emitted discrete dislocations in the plastic zones. $\tau[\Delta_r]$ is the cohesive shear stress,

$$\tau[\Delta_r] = \tau_{max} \sin\left(2\pi \frac{\Delta_r}{b}\right)$$

For the ith emitted dislocation in the upper plastic zone, we have

$$\tau_{r\theta}^{(0)}(r_i) + A\int_0^R g(r_i, s) b_r(s)\, ds + Ab \sum_{j=1}^{n} g(r_i, r_j) + Ab[g_0(r_i, r_i) + g_1(r_i, r_i)]$$
$$= \tau_f, \quad i = 1, 2, \ldots, N_d \qquad (38)$$

where

$$g(r, s) = \frac{2}{r-s} + g_0(r, s) + g_1(r, s)$$

The functions $g_0(r, s)$ and $g_1(r, s)$ can be extracted from Lin and Thomson (1986).

The calculations were carried out with materials parameters

$$\frac{h}{b} = 1.0, \quad \nu = 0.3, \quad \frac{\tau_0}{\mu} = 0.02, \quad \frac{\tau_f}{\mu} = 0.002, \quad \frac{\tau_{max}}{\mu} = 0.1596, \quad \alpha = 45^\circ \quad \text{and} \quad M = 120$$

Figure 16(a) shows variation of local stress intensity factor K_I^{tip} vs δ_r^{tip} before dislocation emission. Figure 16(b) shows variation of local stress intensity factor K_I^{tip} vs $\Delta_r^{tip}/b - N_d$ after the N_dth dislocation emission. A dislocation is presumed to be emitted from the crack tip region when K_I^{tip} reaches the maximum value.

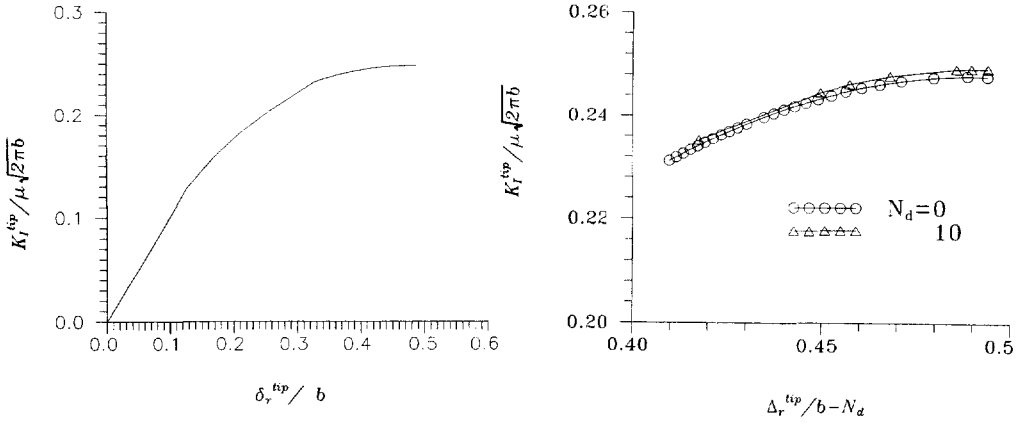

Fig. 16. Local stress intensity factor variation: (a) K_I^{tip} vs δ_r before dislocation emission; (b) K_I^{tip} vs $\Delta_I^{tip}/b - N_d$ after the N_dth dislocation emission.

The relation between the local stress intensity factor K_I^{tip} the applied stress intensity factor K_I is shown in Fig. 17. At the first stage, K_I^{tip} is identical to K_I before any dislocation emission. At point A_0, the local stress intensity factor K_I^{tip} reaches the critical value $K_{Ie}^{(0)}$, then the first nucleated dislocation is emitted away from the crack tip region and stopped at distance $r = r_{ob}$. The K_I^{tip} is decreased from point A_0 to B_1 along a vertical line A_0B_1. Since the emitted dislocation escapes rapidly from the crack tip with high speed, so that the applied stress intensity K_I can be considered keeping constant during the dynamic process of dislocation emission.

As the applied stress intensity increases again, the K_I^{tip} will increase along the straight line B_1A_1. At point A_1, the local stress intensity factor K_I^{tip} achieves a critical value $K_{Ie}^{(1)}$, which is only a little bit larger than $K_{Ie}^{(0)}$, the second dislocation will move out of the crack tip region and stop at distance r_2. Then the local stress intensity factor K_I^{tip} drops from point A_1 to point B_1 due to shielding by the second emitted dislocation.

The $K_{Ie}^{(1)}$ is the maximum value of K_I^{tip} in a curve of K_I^{tip} vs $(\delta_r^{tip}/b-1)$ after the first dislocation emission. As the sequence is repeated, at point A_N, the K_I^{tip} is exceeded the K_I^{intrin}, cleavage will occur before the next dislocation emission. Here the K_I^{intrin} is the intrinsic fracture toughness of a dislocation free material.

If the value of the K_I^{intrin} is high enough, there is another possibility: the local stress intensity factor reaches the terminal value K_I^{term}, which is determined by $L_{DFZ} < b$. Here L_{DFZ} is the length of DFZ. In such kind situation, the crack tip will be fully shielded by the dislocation emission and cleavage is prevented. As pointed out by Zhu *et al.* (1996), the dislocation nucleation process may be terminated also by the nanocrack nucleation ahead of the crack tip. Thus, the nanocrack coalesces to the main crack.

The applied stress intensity factor K_I vs the number N_d is plotted in Fig. 18. The dashed line between points A_{i-1} to B_i represents the dynamic process of the ith dislocation emission. The solid vertical line B_iA_i denotes the loading process after the ith dislocation emission. Figure 19 shows the upper envelope of the actual curve of the applied stress intensity factor K_I vs the total number N_d of the emitted dislocations. A corresponding upper envelope curve for K_I^{tip} is shown in Fig. 20. We should emphasis that the upper envelope of the local stress intensity K_I^{tip} increases very slowly with the increase of the total number N_d, meanwhile the upper envelope of the applied stress intensity factor K_I increases rapidly.

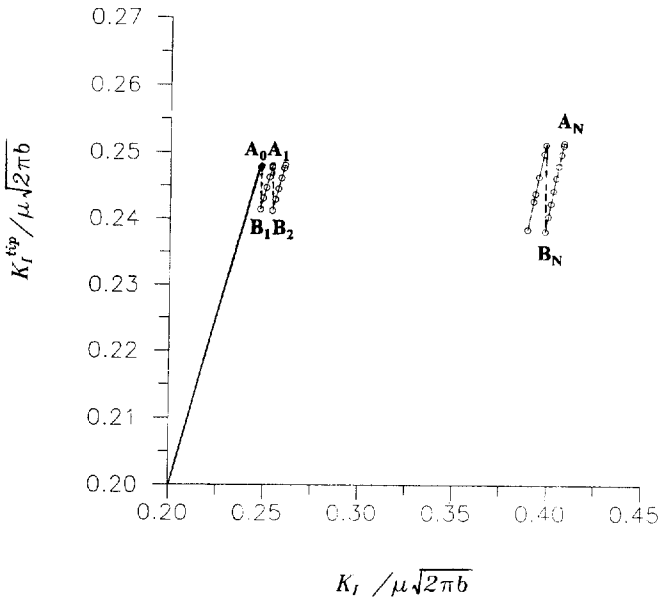

Fig. 17. Local stress intensity factor K_I^{tip} vs applied stress intensity factor K_I.

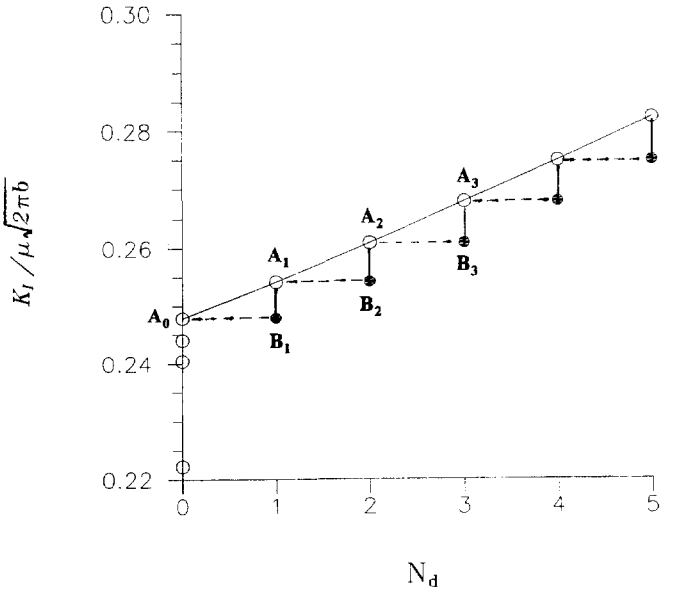

Fig. 18. Applied stress intensity factor K_I as a function of the total number N_d of the emitted dislocations.

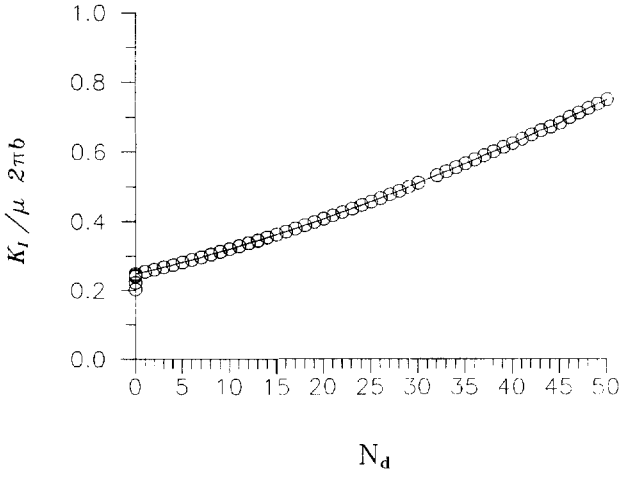

Fig. 19. Upper envelope of applied stress intensity factor K_I vs the total number N_d of the emitted dislocations.

7. DISCUSSION

A unified model for dislocation nucleation, emission and dislocation free zone is proposed in the this paper based on the Peierls framework and with a slight modification of the Rice's concept. Three regions are identified ahead of the crack tip, that is, the cohesive zone immediately ahead of the crack tip, the plastic zone formed by the emitted discrete dislocations which are located out of the crack tip area and a dislocation free zone between those two zones.

It is shown by the calculation results that the stress distribution immediately ahead of the crack tip is mainly determined by local stress intensity factors which are characterized by the parameters R_1 and R_2. The effect of the number N_d of the emitted dislocations on the near tip stress fields is small, if the deformation state near the crack tip is stable. But the applied stress intensity factor K_{II} is nearly proportional increase as the total number N_d of the emitted dislocations increases.

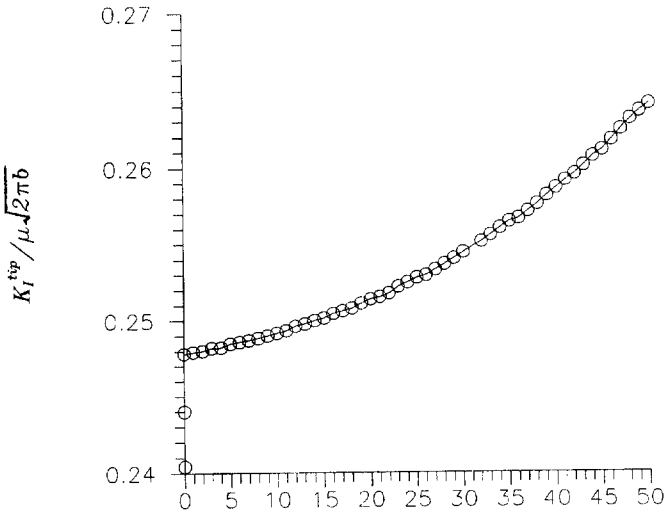

Fig. 20. Upper envelope of local stress intensity factor K_I^{tip} vs the total number N_d of the emitted dislocations.

If the total number N_d of the emitted dislocations is large enough (i.e. the applied stress intensity factor K_{II} big enough) the deformation state ahead of the crack tip becomes unstable, which results in continuously dislocation emission and completely dislocation shielding on the crack tip. Finally whole interval $[0, x_{ob}]$ is transformed to the plastic zone and the dislocation free zone vanishes.

If the material is a perfect crystal without any obstacle, then the emitted dislocations will stop at distances about 5–10 μm magnitude when the lattice friction $\tau_f/A = 0.005$.

It should be pointed out that the present analysis concerns only a two-dimensional description, while it is evident that the dislocation emission actually takes place in a three-dimensional geometry by a dislocation loop. The elastic anisotropy and the effect of the thermal activation on the dislocation are also neglected in the present analysis. Further investigation is needed.

Acknowledgements—This research is supported by the Chinese National Natural Science Foundation. The author is grateful to Prof. K. R. Wang for reviewing the manuscript.

REFERENCES

Beltz, G. E. and Rice, J. R. (1991) In *Modeling the Deformation of Crystalline Solids*, ed. C. L. Teery *et al.*, p. 457. The Mineral, Metal Material Society.
Chiao, Y. H. and Clark, D. R. (1989) *Acta Metallica* **37,** 203.
Dai, S. H. and Li, J. C. M. (1982) *Scripta Met.* **16,** 183.
Erdogan, F. and Gupta, G. D. (1982) *Quarterly Applied Mathematics* **1**(1972), 525.
Horton, J. A. and Ohr, S. M. (1982) *Scripta Metal.* **16,** 621.
Li, J. C. M. (1981) In *Dislocation Modelling Physical Systems*, ed. M. F. Ashby *et al.*, p. 498. Pergamon, N.Y.
Lin, I. H. and Thomson, R. (1986) *Acta Metallica* **34,** 187.
Loo, K. K. (1987) *Journal of Applied Mechanics* **45,** 797.
Ohr, S. M. (1985) *Mater. Sci. Eng.* **72,** 1.
Rice, J. R. and Thomson, R. M. (1974) *Philosophical Magazine* **29,** 73.
Rice, J. R. (1992) *Journal of the Mechanics and Physics of Solids* **40,** 239.
Rice, J. R., Beltz, G. E. and Sun, Y. (1992) In *Topics in Fracture and Fatigue*, ed. A. S. Argon, p. 1. Springer-Verlag.
Schoeck, G. (1991) *Philosophical Magazine* **63,** 111.
Wang, T. C. (1995) *International Journal of Fracture* **69,** 295.
Zhu, T., Yang, W. and Guo, T. (1996) *Acta Metallica* **44,** 3049.